European Polymer Journal 174 (2022) 111337

Contents lists available at ScienceDirect

European Polymer Journal

journal homepage: www.elsevier.com/locate/europolj

Novel hybrid organic/inorganic poly(thiourethane) covalent adaptable networks

Federico Guerrero [a], Silvia De la Flor [b,*], Xavier Ramis [c], José-Ignacio Santos [d], Angels Serra [a,*]

[a] Dept. of Analytical and Organic Chemistry, Universitat Rovira i Virgili, C/ Marcel·lí Domingo, Edif. N4., 43007 Tarragona, Spain
[b] Dept. of Mechanical Engineering, Universitat Rovira i Virgili, Av. Països Catalans, 26, 43007 Tarragona, Spain
[c] Thermodynamics Laboratory, ETSEIB Universitat Politècnica de Catalunya, Av. Diagonal, 08028 Barcelona, Spain
[d] Joxe Mari Korta Center, NMR Facility, SGIKER-UPV/EHU, C/ Tolosa Hiribidea, 72, 20018 Donostia, Spain

ARTICLE INFO

Keywords:
Vitrimers
Poly(thiourethane)
Thermosets
POSS
Click reaction

ABSTRACT

Organic-inorganic hybrid materials combine the advantages of both phases: hardness and strength of inorganic phase and elasticity and toughness of the organic matrix. In the present study, we have prepared nanocomposites with a poly(thiourethane) polymeric matrix and silsesquioxane-type structures, with thiols as reactive groups (POSS-A or POSS-B, synthesized in different pressure conditions), looking for a covalent interaction between both phases, and good dispersion. Due to the *click* behavior of the reaction between the isocyanate and the thiol groups, highly homogeneous materials are obtained. Both monomers, catalyst (dibutyltin dilaurate, DBTDL), and the POSS precursor (3-mercaptopropyl trimethoxysilane, MPTMS), are commercially available, which present the advantage of being industrially scalable. The incorporation of POSS leads to an increase in glassy and rubbery storage moduli and the temperature of the maximum of tan δ curve. The vitrimeric behavior of the poly(thiourethanes) improved with the POSS incorporation, getting lower relaxation times. With a higher proportion of closed cages, POSS-B leads to the most significant improvements. All the materials prepared showed high transparency and the fracture of POSS modified materials indicates an improved toughness.

1. Introduction

In this century, the need to recycle thermosets residues to improve the sustainability of our planet has led a large number of researchers to develop new materials with these capabilities. As early as 1946, Tobolsky *et al.* [1] reported an unexpected behavior of some types of cross-linked polymers when changing the temperature, which allows these materials to maintain their mechanical and thermal performance but acquire the processability of thermoplastics. These materials, whose topology can be changed by thermally activated reversible chemical processes, are nowadays known as covalent adaptable networks (CANs) [2,3], being vitrimers included in the CANs group. These reversible reactions allow the reprocessing and recycling of cross-linked polymers and can exhibit other characteristics as self-healing or self-welding properties [4].

Among the thermosets that can be included in the group of CANs, poly(urethane)s have been deeply studied [5,6]. Polyurethanes (PUs) are of great economic importance since they are one of the most consumed thermosets (around 5 % of polymers total production in the world) with applications such as coatings, adhesives, foams, and elastomers [7,8]. Their thiol analogous, poly(thiourethane)s or poly(thiocarbamate)s (PTUs), can present several advantages over them. For example, they can be prepared by a click-reaction between isocyanates and thiols, with high conversions and without by-products as allophanates, formed during PU preparation, creating homogeneous networks [9]. In addition, poly(thiourethane)s are biocompatible and have excellent optical properties [10,11]. Recently, we have developed poly(thiourethane) materials with vitrimer-like properties and demonstrated their easiness of recycling and reshaping [12,13,14]. CANs based on PTUs have also been reported by other research teams in low T_g cross-linked materials [15,16].

Hybrid organic–inorganic materials were introduced as one of the strategies to improve mechanical properties and obtain new high-performance polymeric materials. Hybrid materials present a synergism that meets the advantages of both organic and inorganic phases: hardness and strength of inorganic phase, and elasticity and toughness of the organic matrix [17]. There are two different ways of preparing this type of material. The first one is through the sol–gel process, which

* Corresponding authors.
E-mail addresses: silvia.delaflor@urv.cat (S. De la Flor), angels.serra@urv.cat (A. Serra).

https://doi.org/10.1016/j.eurpolymj.2022.111337
Received 24 March 2022; Received in revised form 2 June 2022; Accepted 5 June 2022
Available online 8 June 2022
0014-3057/© 2022 The Author(s). Published by Elsevier Ltd. This is an open access article under the CC BY license (http://creativecommons.org/licenses/by/4.0/).

allows the *in-situ* formation of the inorganic phase by the so-called bottom-up approach [18,19,20]. The second system is the addition of nano blocks to the matrix or the initial formulation [21], also known as the top-down approach. Inorganic nanoscale building blocks include graphene, nanotubes, layered silicates, metal nanoparticles, etc., among which silica structures and silsesquioxanes (POSS) are viewed as one of the most exciting nanofillers [22]. If nano blocks have reactive groups, they can become covalently linked to the polymeric matrix, which helps to improve the dispersion of these structures and increase the interphase interaction, improving some characteristics of the nanocomposites, especially their mechanical performance. Because of the nanoscale dimensions of POSS and several silica structures, the light scattering of homogeneous materials can be avoided, and the optical transparent nanocomposite materials are suitable for optical applications. The addition of nano blocks to reactive formulations is much easier than the *in-situ* sol–gel process since in the latter, small amounts of water are needed to perform the reaction, and alcohol molecules are always formed, which sometimes leads to the appearance of bubbles in the thermoset. In addition, hydrolyzable monomers like isocyanates can lead to undesirable side reactions if water is added to the initial formulation.

In the present study, we have investigated the effect of reinforcing poly(thiourethane) CANs with thiol-functionalized silica nanostructures. The aim is to achieve a good dispersion of the inorganic structures in the polymeric matrix while improving thermomechanical characteristics. Therefore, thiol-isocyanate formulations with increasing amounts of thiol terminated inorganic SiO_2 structures have been cured, and the curing process has been followed by calorimetric and FTIR studies. The formulations are formed by hexamethylene diisocyanate (HDI), the thiol-functionalized silica nanostructure (named POSS), and trimethylolpropane tris(3-mercapto propionate) (S3) in stoichiometric isocyanate/thiol ratio, using dibutyltin dilaurate (DBTDL) as the catalyst. We have synthesized two different nanosilica structures by condensation of 3-mercaptopropyl trimethoxysilane (MPTMS) in acetone/acidic water solutions at atmospheric pressure (POSS-A) and under autogenic pressure (POSS-B). Both oligomeric silica structures have thiols as reactive groups, but the use of pressure favors the formation of a higher proportion of POSS cages, and therefore, the silica reinforcements have different morphology.

Various articles describe the behavior of silica-reinforced elastomeric CANs. Legrand *et al.* [23] reported the effect of reactive and non-reactive silica nanoparticles in epoxy composites. They observed an increased modulus in the glassy and rubbery state but a slowdown in stress relaxation. Surface exchangeable bonds speed up the relaxation of composites compared to nonfunctionalized filler and allow better dispersion in the matrix. Barabanova et al. [24] demonstrated that silica nanoparticles enhance the welding ability of epoxy-anhydride vitrimers and increase the topology freezing temperatures. Yang et al. [25] added epoxy functionalized POSS to an epoxy-acid formulation. The vitrimeric composites improved their mechanical characteristics compared with the virgin material and were easily recycled. However, they relaxed the stress more slowly. Torkelson and co. [26] reported elastomeric reprocessable poly(hydroxyurethane) composites. Whereas when non-reactive silica nanoparticles are used, the material is able to recover its cross-link density completely after a reprocessing step. Contrarily, functionalized nanoparticles with groups that can participate in dynamic chemistries lead to losses in mechanical properties associated with the cross-link density at working temperatures, along with faster rates and lower apparent activation energies of stress relaxation at higher temperatures. Elastomeric vitrimers with mechanical robustness, malleability, and recyclability were described by Guo *et al.* [27] based on the effect of surface silanol moieties. Silica played the role of reinforcement and cross-linker to endow the networks with chemical and mechanical robustness. Moreover, these permanent networks can reshuffle the topological structure upon temperature-induced *trans*-oxyalkylation reactions in the elastomer-silica interphase.

As far as we know, the present study is the first to address the role of two different oligomeric silica structures, with more or less content in POSS boxes, as nanofillers in the vitrimeric-like behavior of poly(thiourethane)s with high T_g and excellent characteristics as thermosetting materials. The nanocomposites obtained on varying the proportion of both types of thiol-functionalized silica nanofillers have been characterized from the thermal and mechanical point of view and the relaxation behavior studied by thermomechanical analysis.

2. Experimental part

2.1. Materials

3-Mercaptopropyl trimethoxysilane (MPTMS) from Alfa Aesar. Trimethylolpropane tris(3-mercapto propionate) (S3), hexamethylene diisocyanate (HDI), and dibutyltin dilaurate (DBTDL) from Sigma-Aldrich. Hydrochloric acid, acetone, and chloroform from Scharlab. All the products were used as received.

2.2. Preparation of octathiol silsesquioxane (POSS)

2.2.1. At atmospheric pressure (POSS-A)

Octathiol silsesquioxane (POSS-SH) was prepared according to a reported methodology [28] 13.4 g (68 mmol) of MPTMS precursor and 100 mL of acetone were placed in a flask equipped with reflux and a magnetic stirrer. Then, 17.3 mL of conc. hydrochloric acid and 21 mL of deionized water were added. The molar ratio HCl:MPTMS was 3:1. After 48 h at reflux, a white solid was formed. The solid was washed with cold acetone several times and dried at 60 °C overnight. The resulting product was a white powder with a 92 % of yield. This white powder was ground and sieved through a 0.05 mm sieve.

2.2.2. At autogenic pressure (POSS-B)

The same mixture as in Section 2.2.1 was reacted in a 150 mL autoclave reactor, and after 48 h at 90 °C, an orange solution was formed. This solution was added to cold deionized water, forming a yellowish precipitate. The precipitate was separated by centrifugation (2000 rpm for 10 min). Then, it was solved again in acetone, dried using anhydrous magnesium sulfate, filtered, and the solvent was eliminated using reduced pressure. The product was an orange oil with a 36 % of yield.

2.3. Preparation of the formulations

Formulations were prepared by mixing stoichiometric amounts of isocyanate and thiol groups, and the amount of POSS was calculated in percentage in weight over the mass of S3. Firstly, POSS and S3 are mixed, and then HDI is added and stirred. Finally, the corresponding amount of DBTDL is added. Due to the catalyst's reactivity, even at room temperature, formulations cannot be stored for a long time and were always maintained at cold. The composition of the formulations tested is detailed in Table 1. To 1.58 g (9.4 mmol) of HDI 0.025 g (0.04 mmol) of DBTDL were added in all formulations.

2.4. Sample preparation

The samples were prepared by pouring the formulations on Petri dishes covered with adhesive Teflon to avoid sticking to the glass. The formulations were heated at 140 °C for 30 min to obtain a flexible material able to be removed from the mold, and fully cured in a hot-press at 170 °C for 60 min under a pressure of 15 MPa. The cured samples were die-cut to obtain rectangular specimens of 20 × 5 × 0.5 mm^3.

Table 1
Composition of the formulations studied in gram and the weight percentage.

Formulation	S3		POSS		HDI		DBTDL	
	g	%	g	%	g	%	g	%
0POSS	2.50	60.90	0.00	0	1.58	38.49	0.025	0.61
5POSS	2.38	57.98	0.12	2.92	1.58	38.49	0.025	0.61
10POSS	2.27	55.30	0.23	5.60	1.58	38.49	0.025	0.61
15POSS	2.17	52.86	0.33	8.04	1.58	38.49	0.025	0.61

2.5. Characterization techniques

Solid-state ^{29}Si NMR spectra (^{29}Si CPMAS-NMR) were recorded at 25 °C for the synthesized POSS A and B on a Bruker Advance III 400 MHz at a frequency of 79.5 MHz on a 4 mm MAS DVT TRIPLE Resonance HYX probe. NMR spectra were obtained with 4000 scans using the following parameters: rotor spin rate 10000 Hz, recycling time 5 s, contact time 2.0 ms, and acquisition time 43 ms. Exponential apodization with a line broadening 30 Hz, FT and manual phasing, and baseline correction was used when processing the data.

The thermal stability of the cured samples was evaluated by thermogravimetric analysis (TGA), using a Mettler TGA 2 STAR System thermo-balance. All experiments were performed under synthetic air (flow 50 mL/min). Pieces of 10–15 mg cured samples were degraded between 30 and 600 °C at a heating rate of 10 °C/min.

FTIR spectra were recorded with a spectrometer Jasco FT/IR 6700, with a resolution of 4 cm^{-1}, in an interval from 650 to 4000 $cm^{-1,}$ and 32 scans of each spectrum. The spectrometer was equipped with an accessory Specac Golden Gate ATR Tecknokroma. All spectra were registered at room temperature.

The viscoelastic and thermomechanical properties were evaluated with a DMA Q800 analyzer from TA Instruments and using a film tension clamp. The dependence of tan δ and storage modulus on the temperature was investigated in the initial materials and after several stress relaxations experiments. The samples were tested at a heating rate of 2 °C/min from −25 to 125 °C, with a frequency of 1 Hz and 0.1 % of strain. Tensile stress relaxation tests were conducted using a film tension clamp on samples with the same dimensions as previously defined. The samples were equilibrated at 165 °C and left at this temperature for 5 min. Then, a constant strain of 1.5 % (to ensure the materials are within the linear range) was applied, and the consequent stress level was measured as a function of time for 90 min. Then, the temperature was increased to 5 °C, and the process was repeated until a final temperature of 195 °C was reached. Relaxation stress $\sigma(t)$ was normalized by the initial stress (σ_o), and the relaxation time (τ) was determined as the time necessary to relax $0.37{\cdot}\sigma_o$.

With the relaxation times obtained at each temperature, the activation energy values, E_a, were calculated using an Arrhenius-type equation:

$$\ln(\tau) = \frac{E_a}{RT} - \ln A \quad (1)$$

Where τ is the time needed to attain a stress-relaxation value $(0.37\sigma_0)$, A is a pre-exponential factor, and R is the gas constant. The temperature of topology freezing (T_v) was obtained from the Arrhenius relation as the temperature at which the material reaches a viscosity of 10^{12} Pa·s. Using Maxwell's relation and E' determined from DMA (assuming E' is relatively invariant in the rubbery state), τ^* was determined for each sample. The Arrhenius relationship was then extrapolated to the corresponding value of τ^* to determine T_v for each sample.

Environmental scanning electron microscopy (ESEM) was used to examine the surfaces of the broken materials prepared. A Quanta 600 environmental scanning electron microscopy (FEI Company, Hillsboro, OR, USA) allows collecting micrographs at 10–20 kV and low vacuum mode without the need to coat the samples.

3. Results and discussion

3.1. Preparation and characterization of thiol-functionalized silica nanostructures

Several authors reported the addition of POSS (silsesquioxane) structures as nano blocks to reinforce thermosets [29]. POSS is a three-dimensional nanostructure with the generic formula $\{RSiO_{3/2}\}_n$, where R is an organic moiety. The most extended use of POSS in thermosets has been reported in epoxy materials. In that case, POSS has been functionalized with epoxy [30], amine [31], and hydroxyl groups [32], and the thermosets obtained presented improved toughness, stiffness, thermal stability, and flame retardancy. In addition, polyimides [33], phenolic resins [34], and poly(urethane)s [35,36] have been modified by these structures to improve thermal and mechanical characteristics, among others.

In the present work, we have synthesized oligomeric structures containing POSS cages with thiol groups that are reactive in front of isocyanates producing thiourethane bonds. Thus, the thiol-reactive groups in the POSS nanostructures not only contribute to the miscibility in the organic phase but also lead to crosslinking points due to the high functionality of the POSS structure (eight for perfect POSS cages). The idealized structure for the thiol-functionalized POSS synthesized in this work is depicted in Scheme 1.

The preparation of POSS derivatives can be summarized in a two-step process: the first one is the hydrolysis of a trialkoxysilane, forming silanols, followed by their condensation, which eliminates water. Some factors that must be controlled are the solvent, catalyst, precursor, dilution, time, and temperature [37]. Forming perfectly closed POSS cages is not an easy task and usually coexists with other partially closed structures or even randomly ordered [38].

The synthesis of the two different mercaptopropyl POSS (POSS-A and POSS-B) was performed according to the procedure previously reported [28] and explained in Section 2.2. To improve the formation of POSS cages, POSS-B was synthesized in an autoclave which allows reaching a higher temperature and pressure, which predictably leads to a higher hydrolysis proportion of alkoxysilane groups and a better condensation

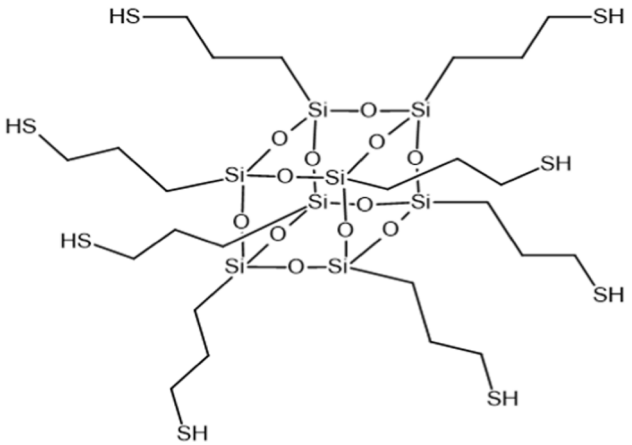

Scheme 1. Idealized structure of the cages of the octathiol POSS synthesized.

of the silanols.

The characterization of POSS structures is usually performed by ^{29}Si-CPMAS NMR spectroscopy. As the MPTMPS precursor has three hydrolyzable groups, different signals attributable to T_n structures can be expected (T_0, T_1, T_2, and T_3) for trisilanols to completely condensed silicon structures. As a general trend, the signals appear at higher chemical shifts on increasing the condensation degree (from T_0 to T_3). This is because cubic cage-like structures reduce the valence angles of Si atoms, and the density of positive charge is reduced. In linear structures or bigger cages, the internal tension is less, and consequently, the signal would be high field shifted. The spectra in Fig. 1 show the presence, for POSS-A and POSS-B samples, of two partially overlapped peaks that correspond to two different chemical environments of the silicon atoms in POSS structures.

According to the values reported in the literature, we assigned the signals at −67 ppm to T_3 that correspond to [$Si(OSi)_3R$] and the signals at −58 ppm to T_2 that correspond to [$Si(OSi)_2R(OH)$] [18,39]. The broadness of both peaks with a partial splitting accounts for a not well-defined oligomeric structure. Although this type of spectra is not quantitative, it is evident in the spectra the differences in both POSS samples prepared by the two different procedures that, in any case, lead to a completely closed structure. The material obtained at autogenic pressure (POSS-B) presents a higher area ratio T_3/T_2 than POSS-A obtained at atmospheric pressure, indicating a more closed structure for POSS-B. In none of the spectra, it was possible to observe signals at chemical shifts in the T_1 and T_0 region, so it can be concluded that the degree of condensation reached has been relatively high.

FTIR spectra can also provide information about the structure of the POSS materials prepared. In Fig. 2, the FTIR spectra show some differences in the absorption bands at 1100 cm^{-1} (stretching of Si-O-Si in the cage structure) and at around 1010 cm^{-1} (stretching of the Si-O-Si bond of silica network), being the former more intense in POSS-B [40].

In the spectrum of POSS-B (autogenic pressure), the relative intensity of the Si-O-Si band is higher than in the case of POSS-A (atmospheric pressure). Therefore, by this technique, a higher proportion of cage POSS structures can be confirmed in POSS-B than in POSS-A, as it was observed by ^{29}Si-CPMAS NMR spectroscopy.

3.2. Study of the curing process

The curing process of the formulations with the highest amount of both POSS synthesized was followed by differential scanning calorimetry (DSC) and compared with the evolution of the neat formulation. Calorimetric curves are shown in Fig. 3, and the most relevant data are presented in Table 2. As we can see, the incorporation of POSS delays the curing process, increasing the temperature at which the curve reaches the maximum. This effect is more pronounced in the case of formulation containing POSS-B. From the values of enthalpy measured, it is confirmed that the covalent union between the inorganic phase and the polymeric matrix has taken place, favoring the interphase interactions and helping the dispersion of the inorganic filler in the PTU matrix.

After the curing process, the FTIR-ATR spectra of cured samples of all three formulations were registered to confirm that the complete curing was reached. The spectra of these samples are shown in Fig. 4. In the spectra, it is possible to observe that the absorption band of isocyanate stretching at 2250 cm^{-1} has practically disappeared and the small remaining absorption could be explained by the topological restrictions produced on curing that hinder the reaction between thiol and isocyanate groups. The weakness of the thiol absorptions does not allow to follow its evolution. We can also observe, that the absorption bands of thiourethane stretching at 1650 cm^{-1} and N-H stretching at 3330 cm^{-1} have been formed. From this technique, no differences are observed among neat and modified formulations, confirming that a fully cured material is obtained and that the differences observed by calorimetric studies are too small to be considered. The main differences observed are

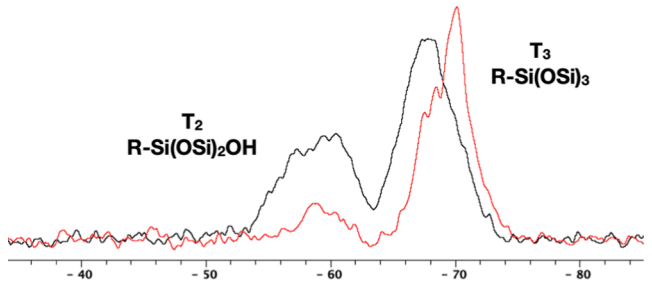

Fig. 1. ^{29}Si-CPMAS NMR spectra of the two POSS-A (black) and POSS-B (red) synthesized.

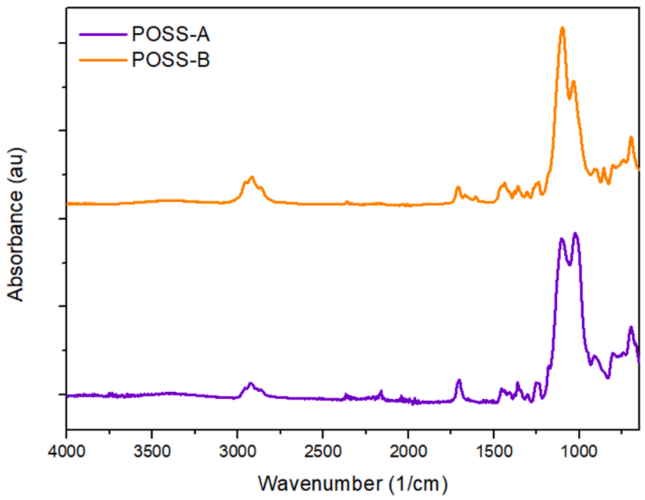

Fig. 2. FTIR spectra of the different thiol-functionalized POSS synthesized.

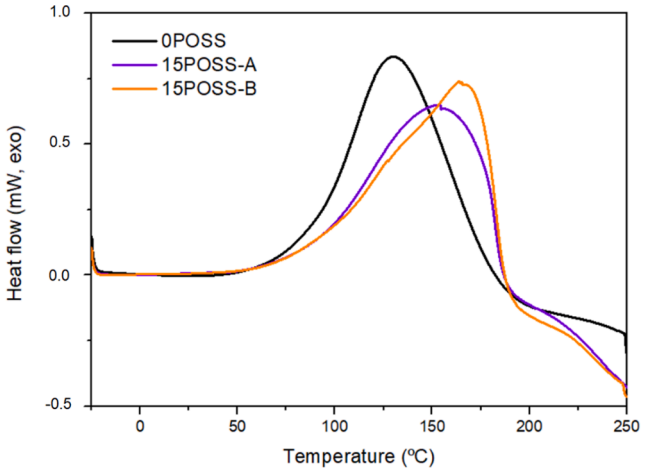

Fig. 3. Calorimetric curves of neat and filled formulations with a 15 % of POSS added.

Table 2
Main calorimetric data of the curing process of neat and modified formulations.

Formulation	T_{max} [a] (°C)	ΔH [b] (J/g)	ΔH [c] (kJ/eq)
Neat	131	353	76
15POSS-A	154	307	67
15POSS-B	164	330	72

[a] Temperature of the maximum of the curing exothermic curve.
[b] Enthalpy released on curing by a gram of formulation.
[c] Enthalpy released on curing by an equivalent of isocyanate or thiol.

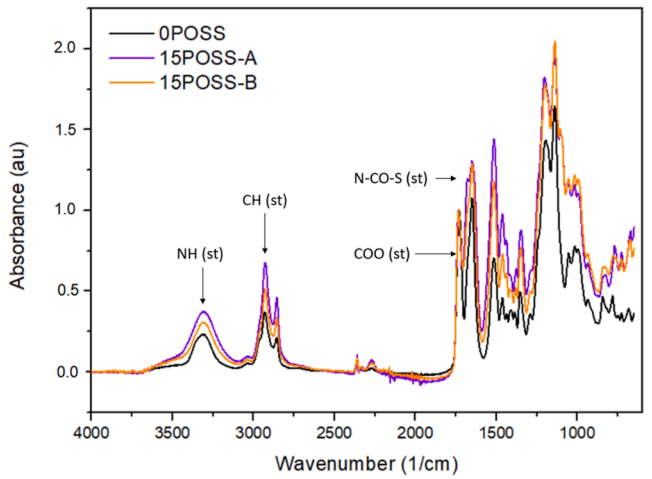

Fig. 4. FTIR spectra of the neat cured material and the nanocomposites with the maximum amount of POSS added.

related to the O-Si-O region with peaks at 1030 and 1100 cm^{-1} due to the presence of POSS in the filled materials.

3.3. Thermal characterization of the nanocomposites

The thermal stability of the materials prepared was evaluated by thermogravimetry (TGA). Fig. 5 shows the first derivative of the weight loss and the most interesting data are presented in Table 3.

As shown in Fig. 5, the degradation occurs in three steps, as previously reported by us [13] for PTUs with different chemical structures. The addition of POSS to the formulation does not change the degradation mechanism, and the three peaks (more or less overlapped) are still present. The first peak can be attributed to the thiourethane group decomposition and the second peak to the β-elimination process of the ester groups in the S3 structure, being the peak at the highest temperature produced by the complete degradation of the network. From the table values, we can see that on increasing the proportion of POSS in the material the initial weight loss starts at a lower temperature. This behavior is more evident in POSS-A due to the presence of terminal groups in the more open silica network. As expected, the char yield at 600 °C determined in the air atmosphere increases with the amount of silicon in the material.

Table 3
Main data obtained from TGA evaluation of the neat material and of the nanocomposites prepared in air atmosphere.

Sample	$T_{5\%}$[a] (°C)	Residue[b] (%)	T_{peak1}[c] (°C)	T_{peak2}[c] (°C)	T_{peak3}[c] (°C)
0POSS	283	2.1	301	327	443
5POSS-A	271	3.8	294	310	454
5POSS-B	282	3.3	301	330	447
10POSS-A	255	5.2	285	310	455
10POSS-B	279	4.8	302	329	454
15POSS-A	247	6.2	279	308	456
15POSS-B	276	5.7	301	330	456

[a] Temperature of 5% of weight loss.
[b] Char residue at 600 °C.
[c] Temperature of the maximum rate of degradation of three main steps.

3.4. Morphological characteristics

The samples' transparency was observed to analyze the dispersion of both POSS structures in the polymeric matrix. Fig. 6 presents the photograph of the neat material and with the highest POSS proportions confirming a proper dispersion.

To analyze the effect of the addition of POSS in the microstructure, the fracture surface of the neat, 15% POSS A, and 15% POSS B were observed after being broken in liquid nitrogen. Fig. 7 presents the SEM images taken at 800 magnifications. It can be seen that the neat sample presents a smooth and uniform surface with few signs of roughness typical of a brittle fracture. Contrarily, the fracture surfaces of both POSS nanocomposites show significant increases in roughness with numerous fracture paths and river-line crack propagation lines distributed uniformly, indicating a more ductile behavior. This surface morphology implies that, in POSS materials, higher energy should be

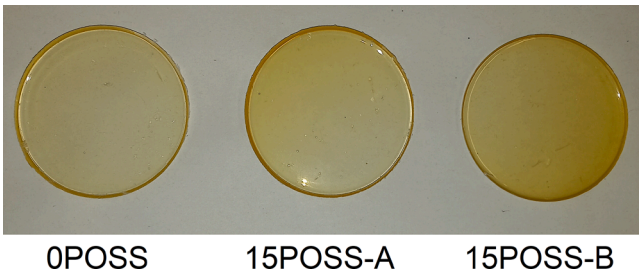

Fig. 6. Photographs of the neat material and with the highest proportion of POSS-A and POSS-B.

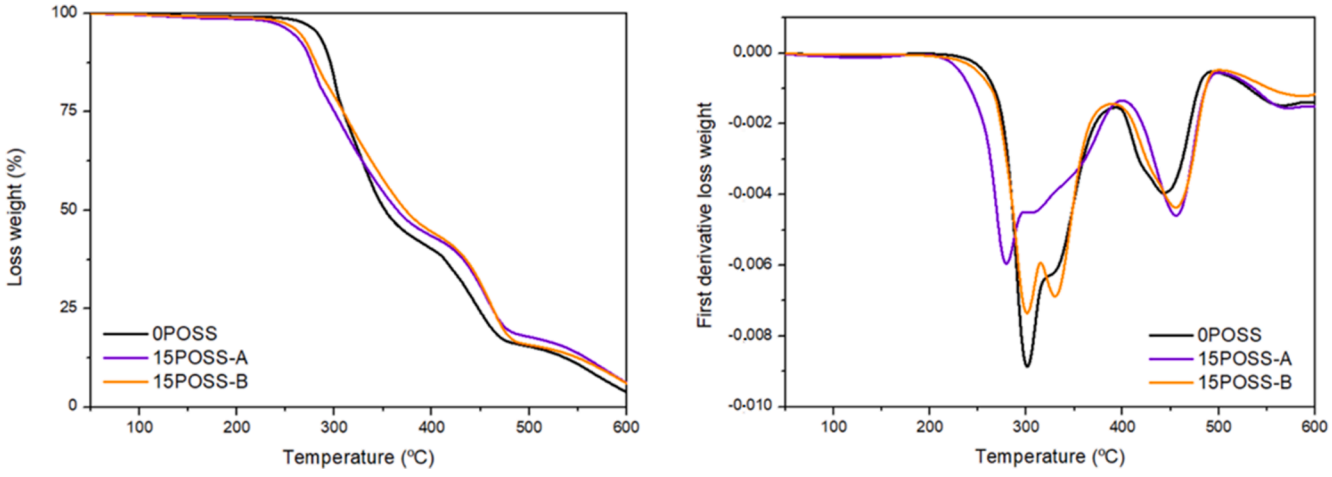

Fig. 5. TGA and DTG curves of the neat cured material and the nanocomposites with the maximum amount of both POSS added.

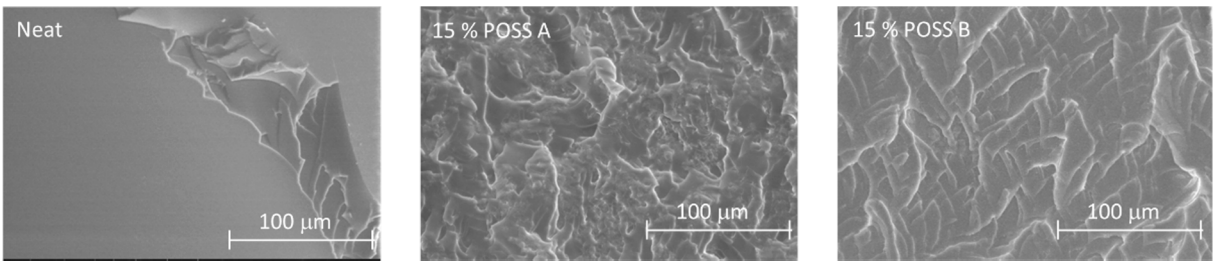

Fig. 7. SEM micrographs of the fracture surfaces of the neat sample and with the highest proportions of POSS tested at 800 magnifications.

consumed for the progress of the cracks, thus presenting higher toughness.

3.5. Thermomechanical properties of the nanocomposites

Dynamic mechanical thermal analysis (DMTA or simply DMA) has been performed to evaluate the materials prepared and the influence of the POSS proportion on their thermomechanical properties. The tan δ curves of all the materials prepared are shown in Fig. 8, and the primary data extracted from the DMA analysis are collected in Table 4.

Looking at the tan δ plots of the neat sample and the nanocomposites prepared with increasing amounts of POSS, it can be observed that the tan δ peaks shift to higher temperatures when rising the proportion of POSS in the material increasing around 20 °C for the highest proportion of POSS added and due to the higher crosslinking density achieved. At the same time, the curves become broader and lower, leading to lower values of tan δ and higher values of FWHM (full width at half maximum), indicating a less homogeneous material with lower damping properties. It is evident that the presence of POSS in the material reduces the mobility of the polymer chains, due to the covalent bonding of the POSS, with a high functionality, to the matrix. This effect is more evident in POSS-A samples, probably due to the more heterogeneous structure of this POSS.

Concerning the values for the storage modulus presented in Table 4, the incorporation of POSS positively affects the stiffness of the materials, increasing both the glassy and rubbery moduli. This increase in stiffness is also due to the increase in the crosslinking density, due to the covalent incorporation of the POSS (with functionality of eight) into the matrix. In general, POSS-B affects more positively due to its more closed structure.

To determine the vitrimeric-like characteristics and to analyze the effect of the proportion of POSS in these nanocomposites, the relaxation behavior was evaluated by DMA stress relaxation tests at different temperatures from 170 °C to 190 °C during 90 min. Fig. 9 shows the normalized stress relaxation of the prepared materials at 180 °C.

Table 4
Primary data obtained from DMA analysis of the neat material and of all the nanocomposites prepared.

Sample	$T_{tan\delta}$ [a] (°C)	*FWHM*[b] (°C)	E'_{glassy}[c] (MPa)	$E'_{rubbery}$[d] (MPa)
0POSS	55	11	2087	10
5POSS-A	59	13	2120	17
5POSS-B	58	13	2195	15
10POSS-A	64	16	2203	23
10POSS-B	67	14	2380	18
15POSS-A	72	26	2295	28
15POSS-B	73	16	2637	23

[a] Temperature at the maximum of the tan δ peak at 1 Hz.
[b] Full width at half maximum of the tan δ peak.
[c] Glassy storage modulus determined by DMA at $T_g - 50$ °C.
[d] Rubbery storage modulus determined by DMA at $T_g + 50$ °C.

As observed in Fig. 9, the incorporation of POSS to the network positively affects the relaxation time, reducing it. Moreover, POSS-B has a more significant effect on the relaxation phenomena than POSS-A. The same tendency was observed in all the temperatures tested. As demonstrated by our research team, the relaxation of PTUs is due to the *trans*-thiocarbamoylation reaction between thiourethane bonds [12,13,14]. This mechanism goes through the decomposition of thiourethanes to isocyanate and thiol, which instantaneously react to form again the thiourethane group. Therefore, the mechanism is dissociative, but with a relaxation behavior typical of vitrimers involving an Arrhenius-type decrease in viscosity as if the degree of crosslinking remained unchanged. These materials with those characteristics can be qualified as vitrimeric-like.

It has been described that an increase in the rubbery modulus reduces the relaxation time because of the decreased ability of reactive groups to diffuse within a higher crosslinked network [41]. However, in the present study, the addition of POSS shortens the relaxation times

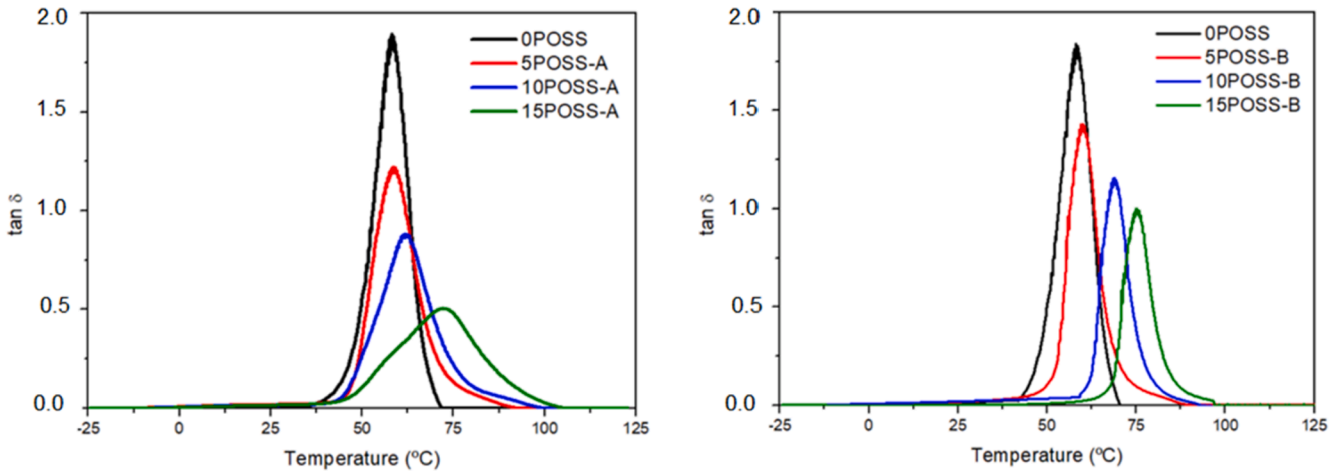

Fig. 8. Evolution of tan δ with the temperature of the neat material and nanocomposites prepared.

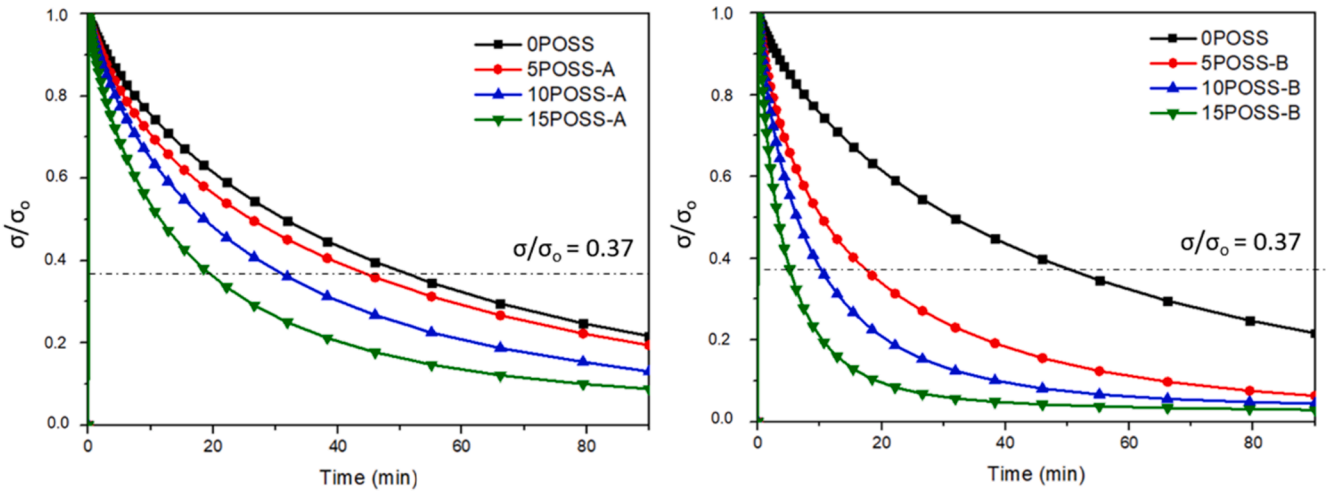

Fig. 9. Normalized stress relaxation plots as a function of time for the different samples obtained with POSS-A (left) and POSS-B (right) at 180 °C.

while producing a significant increase in the rubbery modulus. Silyl ether metathesis has been reported as a mechanism of network relaxation catalyzed by Brönsted or Lewis acids [42]. More recently [43], POSS nanocomposites obtained from polyethylene have been prepared, and it was demonstrated that these thermoplastics could be converted into vitrimers through the introduction of POSS structures and further crosslinking by silyl ether metathesis catalyzed by zinc triflate. Moreover, by measures of refractive index and dielectric properties the structural change on heating poly(silsesquioxane) films has been proved [40]. Thus, in our work, incorporating silsesquioxane structures can provide a second mechanism of relaxation that can potentiate the *trans*-thiocarbamoylation mechanism of the thiourethane groups in the organic matrix shortening the times needed for relaxation.

In previous studies, other research teams have also incorporated two different types of covalent dynamic crosslinking mechanisms [44] such as transesterification and disulfide metathesis [45] and transcarbamoylation and disulfide metathesis [46]. They observed a significant acceleration of the stress relaxation and a decrease in the temperature at which the vitrimer starts to be malleable compared to a similar network with only one exchange mechanism.

From the relaxation stress tests performed at different temperatures between 165 °C and 195 °C, the time to reach a relaxed stress state of $\sigma/\sigma_o = 0.37$ ($\tau_{0.37}$) can be extracted, plotted versus 1/T, and fitted to the Arrhenius relationship (Eq. (1)). From the Arrhenius equation and the relaxation time needed to attain a viscosity of 10^{12} Pa·s, T_v is also calculated for each material. The main parameters from the Arrhenius equation are presented in Table 5 as well as T_v and $\tau_{0.37}$ at 180 °C for each material.

As we can see, there is a noticeable decrease in the $\tau_{0.37}$ values on adding increasing proportions of POSS, leading to the addition of POSS-B to shorter times than POSS-A. The addition of 15 % of POSS-B leads to a relaxation rate around ten times faster than in the case of the neat poly (thiourethane) matrix. It should be considered that the amount of thiourethane bonds in our system is the same despite the composition. However, the activation energies increase on adding POSS to the formulation, although POSS-B rends lower values than POSS-A. The activation energy in chemical exchange reactions indicates the sensitivity of the reaction rate (relaxation times) to temperature. Thus, the presence of POSS raises the sensitivity of these nano compounds to temperature variations in the relaxation phenomena, increasing this dependence with increasing the proportion of the inorganic structure in the material. Moreover, faster relaxations can be achieved by a proper combination of low E_a and high lnA, as in POSS B nanocomposites.

It is important to highlight that in the literature there are no references on the effect of the inorganic network structures in the relaxation process, but it seems evident from the results that the higher proportion of cages in POSS-B favors this relaxation phenomenon.

Regarding the topology freezing temperature (T_v), it can be deduced that increasing the proportion of POSS barely affects this parameter in any POSS structure. However, POSS B presents slightly lower T_v values than POSS A, probably due to its more closed structure, leading to lower moduli and, consequently, lower relaxation times, as explained before [39]. In all the POSS samples, T_v is well above T_g, ensuring excellent creep resistance over a wide temperature range, especially at service (room) temperature.

In a previous study, we could prove how on increasing the proportion of DBTDL, a notable enhancement of the relaxation rate could be observed [12]. As the present study aimed to determine the effect of the addition of POSS to a poly(thiouretane) matrix, we have only tested formulations with 1 phr of DBTDL since the differences will be more pronounced. However, it is foreseeable that on increasing the proportion of DBTDL in the formulation the relaxation times will be highly reduced in the nanocomposites.

To confirm that the network structure remains unaltered after the relaxation process, we performed a thermomechanical analysis to compare their tanδ evolution with temperature. Fig. 10 presents these comparisons for the neat sample and the higher proportion of both POSS after a relaxation test at 180 °C.

To reaffirm that no changes in the chemical network structure have occurred during the relaxation phenomenon, FTIR spectra were recorded before and after a relaxation test at 180 °C. Fig. 11 compares both spectra for the materials with the highest proportion of POSS-A and POSS-B. As we can see, there are no differences when comparing these spectra, confirming that the chemical structure of the network remains unaltered.

From these tests we can assure that the nanocomposite materials can

Table 5
Main data from DMA analysis of the neat material and of the nanocomposites prepared.

Sample	$\tau_{0.37}$[a] (min)	E_a (kJ/mol)	lnA	r^2	T_v[b] (°C)
0POSS	51	137	28.3	0.995	140
5POSS-A	44	162	35.1	0.997	149
5POSS-B	17	159	35.2	0.997	139
10POSS-A	37	181	40.6	0.990	151
10POSS-B	10	179	41.1	0.994	142
15POSS-A	29	187	42.5	0.993	150
15POSS-B	5	192	44.9	0.997	141

[a] Time to reach a value relative relaxed stress of $\sigma/\sigma_o = 0.37$ at 180 °C.
[b] Topology freezing temperature.

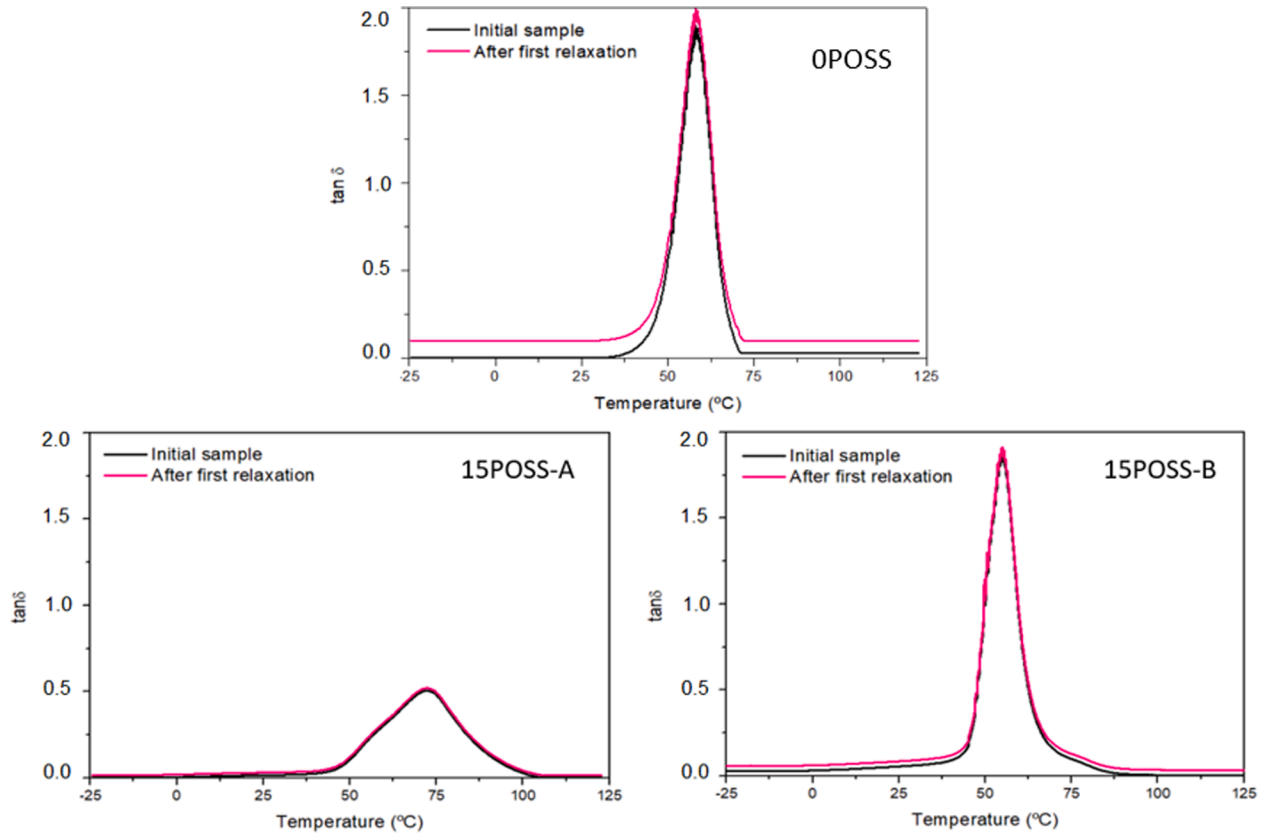

Fig. 10. Comparison of tan δ evolution with temperature before and after a relaxation process at 180 °C for the neat material and with the higher proportion of both POSS.

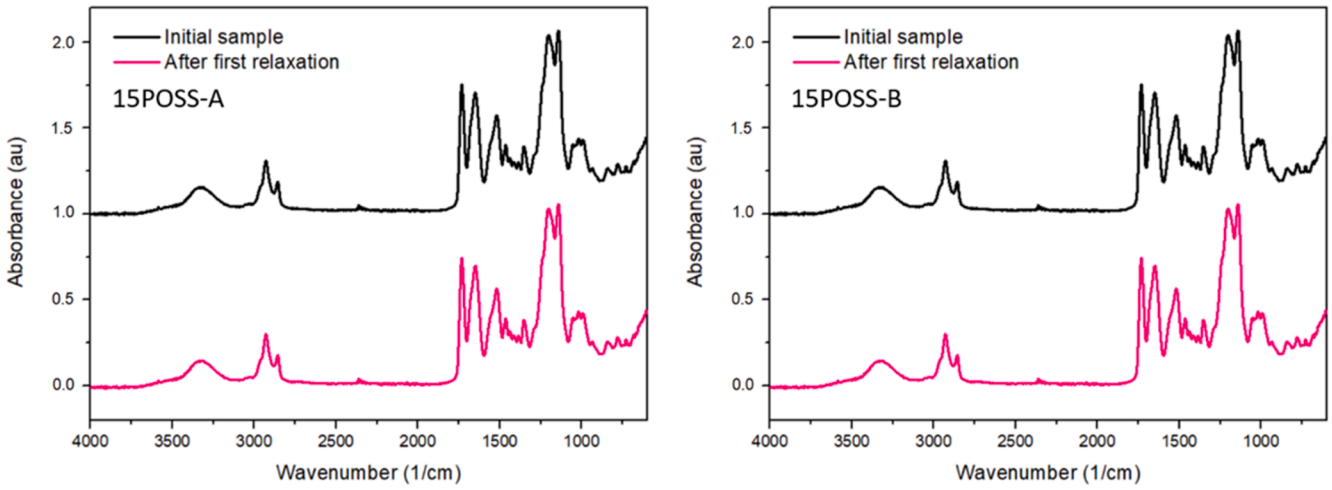

Fig. 11. FTIR spectra for the neat material and the material after relaxation at 180 °C.

be reprocessed without important damage of the network structure and that the presence of silsequioxanes facilitates this process, shortening the time needed.

4. Conclusions

In the present study, hybrid organic–inorganic poly(thiourethane) nanocomposites were prepared from a mixture of a commercial trithiol, different proportions of octathiol functionalized POSS, and hexamethylene diisocyanate. Two POSS derivatives were firstly synthesized by a sol–gel process performed at different conditions: at normal pressure (POSS-A), and in an autogenic autoclave (POSS-B). ^{29}Si NMR spectra showed that POSS-B had a higher proportion of closed octahedral cages. The materials prepared showed good transparency, confirming the excellent dispersion of the inorganic structures in the polymeric matrix.

The presence of POSS in the material led to an increase in the thermomechanical parameters (T_g and storage moduli), although the addition of POSS-A increases the heterogeneity of the material, broadening the tan δ curve. The SEM images of fracture surfaces demonstrated that the addition of POSS makes these nanocomposites more ductile, increasing their toughness.

The addition of POSS leads to a significantly faster relaxation,

especially with a higher proportion of POSS-B, raising the sensitivity to temperature variations in the relaxation phenomena. Contrarily, increasing the proportion of POSS barely affects the topology freezing temperature in any POSS structure, being T_v, in all the cases, well above T_g, ensuring excellent creep resistance over a wide temperature range, especially at service (room) temperature. Comparing the thermo-mechanical and FTIR characteristics before and after a relaxation process at 180 °C, it has been confirmed that the chemical and network structures remain unaltered.

Data availability

The raw data required to reproduce these findings cannot be shared at this time due to technical limitations. Please, contact us in case you need some specific data.

Declaration of Competing Interest

The authors declare the following financial interests/personal relationships which may be considered as potential competing interests: 'Angels Serra reports financial support was provided by Spain Ministry of Science and Innovation.'

Acknowledgments

This work is part of the R&D projects PID2020-115102RB-C21 and PID2020-115102RB-C22 funded by MCINAEI/ 10.13039/501100011033. We acknowledge these grants and the Generalitat de Catalunya (2017-SGR-77 and BASE3D).

References

[1] M.D. Stern, A.V. Tobolsky, Stress-Time –Temperature relations in polysulphide rubbers, J. Chem. Phys. 14 (1946) 93–100, https://doi.org/10.5254/1.3543255.
[2] B.R. Elling, W.R. Dichtel, Reprocessable cross-linked polymer networks: are associative exchange mechanism desirable? ACS Cent. Sci. 6 (2020) 1488–1496, https://doi.org/10.1021/acscentsci.0c00567.
[3] Y. Jin, Z. Lei, P. Taynton, S. Huang, W. Zhang, Malleable and recyclable thermosets: the next generation of plastics, Matter. 1 (6) (2019) 1456–1493, https://doi.org/10.1016/j.matt.2019.09.004.
[4] W. Denissen, J.M. Winne, F.E. Du Prez, Vitrimers: permanent organic networks with glass-like fluidity, Chem. Sci. 7 (1) (2016) 30–38, https://doi.org/10.1039/C5SC02223A.
[5] N. Zheng, Z. Fang, W. Zou, Q. Zhao, T. Xie, Thermoset shape-memory polyurethane with intrinsic plasticity enabled by transcarbamoylation, Angew. Chem. Int. Ed. 55 (38) (2016) 11421–11425, https://doi.org/10.1002/anie.201602847.
[6] D.J. Fortman, J.P. Brutman, C.J. Cramer, M.A. Hillmyer, W.R. Dichtel, Mechanically activated, catalyst-free polyhydroxyurethane vitrimers, J. Am. Chem. Soc. 137 (44) (2015) 14019–14022, https://doi.org/10.1021/jacs.5b08084.
[7] H.-W. Engels, H.-G. Pirkl, R. Albers, R.W. Albach, J. Krause, A. Hoffmann, H. Casselmann, J. Dormish, Polyurethanes: versatile materials and sustainable problem solvers for today's challenges, Angew. Chem. Int. Ed. 52 (36) (2013) 9422–9441, https://doi.org/10.1002/anie.201302766.
[8] J.O. Akindoyo, M.D.H. Beg, S. Ghazali, M.R. Islam, N. Jeyaratnam, A.R. Yuvaraj, Polyurethane types, synthesis and applications-a review, RSC Adv. 6 (115) (2016) 114453–114482, https://doi.org/10.1039/C6RA14525F.
[9] H.C. Kolb, M.G. Finn, K.B. Sharpless, Click chemistry: Diverse chemical function from a few good reactions, Angew. Chem. Int. Ed. 40 (2001) 2004–2021, https://doi.org/10.1002/1521-3773(20010601)40:11<2004::AID-ANIE2004>3.0.CO;2-5.
[10] B. Jaffrennou, N. Droger, F. Méchin, J.-L. Halary, J.-P. Pascault, Characterization, structural transitions and properties of a tightly crosslinked polythiourethane network for optical applications, e-Polym. 082 (2005), https://doi.org/10.1515/epoly.2005.5.1.866.
[11] Y. Jia, B. Shi, J. Jin, J. Li, High refractive index polythiourethane networks with high mechanical property via thiol-isocyanate click reaction, Polymer 180 (2019) 121746, https://doi.org/10.1016/j.polymer.2019.121746.
[12] Gamardella, F. Guerrero, S.D. la Flor, X. Ramis, A. Serra, A new class of vitrimers based on aliphatic poly(thiourethane) networks with shape memory and permanent shape reconfiguration, Eur. Polym. J. 122 (2019), 109361, https://doi.org/10.1016/j.eurpolymj.2019.109361.
[13] F. Gamardella, S. De la Flor, X. Ramis, A. Serra, Recyclable poly(thiourethane) vitrimers with high Tg. Influence of the isocyanate structure, React. Funct. Polym. 151 (2020) 104574, https://doi.org/10.1016/j.reactfunctpolym.2020.104574.
[14] F. Gamardella, S. Muñoz, S. De la Flor, X. Ramis, A. Serra, Recyclable Organocatalyzed poly(thiourethane) covalent adaptable networks, Polymers 12 (2020) 2913, https://doi.org/10.3390/polym12122913.
[15] L. Li, X.i. Chen, J.M. Torkelson, Reprocessable polymer networks via thiourethane dynamic chemistry: recovery of cross-link density after recycling and proof of principle solvolysis leading to monomer recovery, Macromolecules 52 (21) (2019) 8207–8216, https://doi.org/10.1021/acs.macromol.9b01359.
[16] Z. Wen, X. Han, B.D. Fairbanks, K. Yang, C.N. Bowman, Development of thiourethanes as robust, reprocessable networks, Polymer 202 (2020) 122715, https://doi.org/10.1016/j.polymer.2020.122715.
[17] G. Kickelbick, Introduction to hybrid materials, in: G. Kickelbick (Ed.), Hybrid Materials: Synthesis, Characterization, and Applications, Wiley-VCH, Darmstadt, Germany, 2007, pp. 1–48, doi: 10.1002/9783527610495.
[18] A. Serra, X. Ramis, X. Fernández-Francos, Epoxy sol-gel hybrid thermosets, Coatings 6 (1) (2016) 8, https://doi.org/10.3390/coatings6010008.
[19] S. Pandey, S.B. Mishra, Sol–gel derived organic–inorganic hybrid materials: synthesis, characterizations and applications, J. Sol-Gel Sci. Technol. 59 (1) (2011) 73–94, https://doi.org/10.1007/s10971-011-2465-0.
[20] R. Ciriminna, A. Fidalgo, V. Pandarus, F. Béland, L.M. Ilharco, M. Pagliaro, The sol-gel route to advanced silica-based materials and recent applications, Chem. Rev. 113 (8) (2013) 6592–6620, https://doi.org/10.1021/cr300399c.
[21] S. Pavlidou, C.D. Papaspyrides, A review on polymer–layered silicate nanocomposites, Prog. Polym. Sci. 33 (12) (2008) 1119–1198, https://doi.org/10.1016/j.progpolymsci.2008.07.008.
[22] A. Properties, S. Kalia, K. Pielchowski (Eds.), Polymer/POSS Nanocomposites and Hybrid Materials: Preparation, Springer, Cham. Switzerland, 2018.
[23] A. Legrand, C. Soulié-Ziakovic, Silica-Epoxy Vitrimer Nanocomposites, Macromolecules 49 (16) (2016) 5893–5902, https://doi.org/10.1021/acs.macromol.6b00826.
[24] A.I. Barabanova, E.S. Afanas'ev, V.S. Molchanov, A.A. Askadskii, O.E. Philippova, Unmodified silica nanoparticles enhance mechanical properties and welding ability of epoxy thermosets with tunable vitrimer matrix, Polymers 13 (18) (2021) 3040, https://doi.org/10.3390/polym13183040.
[25] H. Yang, C. He, T.P. Russell, D. Wang, Epoxy-polyhedral oligomeric silsesquioxanes (POSS) nanocomposite vitrimers with high strength, toughness, and efficient relaxation, Giant 4 (2020) 100035, https://doi.org/10.1016/j.giant.2020.100035.
[26] X. Chen, L. Li, T. Wei, D.C. Venerus, J.M. Torkelson, Reprocessable polyhydroxyurethane network composites: effect of filler surface functionality on cross-link density recovery and stress relaxation, ACS Appl. Mater. Interfaces 11 (2) (2019) 2398–2407, https://doi.org/10.1021/acsami.8b19100.
[27] S. Wu, Z. Yang, S. Fang, Z. Tang, F. Liu, B. Guo, Malleable organic/inorganic thermosetting hybrids enabled by exchangeable silyl ether interfaces, J. Mater. Chem. A 7 (4) (2019) 1459–1467, https://doi.org/10.1039/C8TA09866B.
[28] I. Penso, E.A. Cechinatto, G. Machado, C. Luvison, C.H. Wanke, O. Bianchi, M.R. F. Soares, Preparation and characterization of polyhedral oligomeric silsesquioxane (POSS) using domestic microwave oven, J. Non-Cryst. Solids 428 (2015) 82–89, https://doi.org/10.1016/j.jnoncrysol.2015.08.020.
[29] J. Zhao, Y. Fu, S. Liu, Polyhedral oligomeric silsesquioxane (POSS)-modified thermoplastic and thermosetting nanocomposites: a review, Polym. Polym. Compos. 16 (8) (2008) 483–500, https://doi.org/10.1177/096739110801600802.
[30] B. Montero, A. Serra, C. Ramírez, X. Ramis, Epoxy/anhydride networks modified with polyhedral oligomeric silsesquioxanes, Polym. Compos. 34 (1) (2013) 96–108, https://doi.org/10.1002/pc.22381.
[31] W.-Y. Chen, Y.-Z. Wang, S.-W. Kuo, C.-F. Huang, P.-H. Tung, F.-C. Chang, Thermal and dielectric properties and curing kinetics of nanomaterials formed from POSS-epoxy and meta-phenylenediamine, Polymer 45 (20) (2004) 6897–6908, https://doi.org/10.1016/j.polymer.2004.07.070.
[32] Z. Zhang, G. Liang, P. Ren, J. Wang, Thermodegradation kinetics of epoxy/DDS/POSS system, Polym. Compos. 28 (6) (2007) 755–761, https://doi.org/10.1002/pc.20341.
[33] C.-M. Leu, Y.-T. Chang, K.-H. Wei, Synthesis and dielectric properties of polyimide-tethered polyhedral oligomeric silsesquioxane (POSS) nanocomposites via POSS-diamine, Macromolecules 36 (24) (2003) 9122–9127, https://doi.org/10.1021/ma034743r.
[34] H.-C. Lin, S.-W. Kuo, C.-F. Huang, F.-C. Chang, Thermal and surface properties of phenolic nanocomposites containing octaphenol polyhedral oligomeric silsesquioxane, Macromol. Rapid Commun. 27 (7) (2006) 537–541, https://doi.org/10.1002/marc.200500852.
[35] B.X. Fu, B.S. Hsiao, H. White, M. Rafailovich, P.T. Mather, H.G. Jeon, S. Phillips, J. Lichtenhan, J. Schwab, Nanoscale reinforcement of polyhedral oligomeric silsesquioxane (POSS) in polyurethane elastomer, Polym. Int. 49 (2000) 437–440, https://doi.org/10.1002/(SICI)1097-0126(200005)49:5<437::AID-PI239>3.0.CO;2-1.
[36] B.X. Fu, B.S. Hsiao, S. Pagola, P. Stephens, H. White, M. Rafailovich, J. Sokolov, P. T. Mather, H.G. Jeon, S. Phillips, J. Lichtenhan, J. Schwab, Structural development during deformation of polyurethane containing polyhedral oligomeric silsesquioxanes (POSS) molecules, Polymer 42 (2) (2001) 599–611, https://doi.org/10.1016/S0032-3861(00)00389-X.
[37] G. Li, L. Wang, H. Ni, C.U. Pittman Jr., Polyhedral oligomeric silsesquioxane (POSS)polymers and copolymers: a review, J. Inorg. Organomet. Polym. 11 (2001) 123–154, https://doi.org/10.1023/A:1015287910502.
[38] H. Mori, M.G. Lanzendörfer, A.H.E. Müller, J.E. Klee, Silsesquioxane-based nanoparticles formed via hydrolytic condensation of organotriethoxysilane containing hydroxy groups, Macromolecules 37 (14) (2004) 5228–5238, https://doi.org/10.1021/ma035482o.
[39] Y. Kaneko, M. Shoiriki, T. Mizumo, Preparation of cage-like octa(3-aminopropyl) silsesquioxane trifluoromethanesulfonate in higher yield with a shorter reaction time, J. Mater. Chem. 22 (2012) 14475–14478, https://doi.org/10.1039/C2JM32355A.

[40] W.-C. Liu, C.-C. Yang, W.-C. Chen, B.-T. Dai, M.-S. Tsai, The structural transformation and properties of spin-on poly(silsesquioxane) films by thermal curing, J. Non-Cryst. Solids 311 (3) (2002) 233–240, https://doi.org/10.1016/S0022-3093(02)01373-X.
[41] J.P. Brutman, D.J. Fortman, G.X. De Hoe, W.R. Dichtel, M.A. Hillmyer, Mechanistic study of stress relaxation in urethane-containing polymer networks, J. Phys. Chem. B 123 (6) (2019) 1432–1441, https://doi.org/10.1021/acs.jpcb.8b11489.
[42] C.A. Tretbar, J.A. Neal, Z. Guan, Direct silyl ether metathesis for vitrimers with exceptional thermal stability, J. Am. Chem. Soc. 141 (42) (2019) 16595–16599, https://doi.org/10.1021/jacs.9b08876.
[43] B. Zhao, G. Hang, L. Li, S. Zheng, Nanocomposites of polyethylene with polyhedral oligomeric silsesquioxane: from thermoplastics to vitrimers through silyl ether metathesis, Mater. Today Chem. 24 (2022) 100759, https://doi.org/10.1016/j.mtchem.2021.100759.
[44] L. Hammer, N.J. Van Zee, R. Nicolaÿ, Dually crosslinked polymer networks incorporating dynamic covalent bonds, Polymers 13 (2021) 396, https://doi.org/10.3390/polym13030396.
[45] M. Chen, L. Zhou, Y. Wu, X. Zhao, Y. Zhang, Rapid stress relaxation and moderate temperature of malleability enabled by the synergy of disulfide metathesis and carboxylate transesterification in epoxy vitrimers, ACS Macro Lett. 8 (3) (2019) 255–260, https://doi.org/10.1021/acsmacrolett.9b00015.
[46] D.J. Fortman, R.L. Snyder, D.T. Sheppard, W.R. Dichtel, Rapidly reprocessable cross-linked polyhydroxyurethanes based on disulfide exchange, ACS Macro Lett. 7 (10) (2018) 1226–1231, https://doi.org/10.1021/acsmacrolett.8b00667.